SKB

TECHNICAL REPORT 88-24

Fission product concentration profiles (Sr, Xe, Cs and Nd) at the individual grain level in power-ramped LWR fuel

R S Forsyth, O Mattsson, D Schrire

Studsvik Nuclear

December 1988

SVENSK KÄRNBRÄNSLEHANTERING AB
SWEDISH NUCLEAR FUEL AND WASTE MANAGEMENT CO

BOX 5864 S-102 48 STOCKHOLM
TEL 08-665 28 00 TELEX 13108-SKB

FISSION PRODUCT CONCENTRATION PROFILES (Sr, Xe, Cs and Nd) AT THE INDIVIDUAL GRAIN LEVEL IN POWER-RAMPED LWR FUEL

R S Forsyth, O Mattsson, D Schrire

Studsvik Nuclear

December 1988

STUDSVIK NUCLEAR

STUDSVIK/NF(P)-88/31

1988-12-19

SKB 1:29

R.S. Forsyth
O. Mattsson
D. Schrire

Fission product concentration profiles (Sr, Xe, Cs and Nd) at the individual grain level in power-ramped LWR fuel.

ABSTRACT

In addition to dissolution of the UO_2 matrix, the corrosion of spent nuclear fuel in groundwater appears to occur, at least in the short term, by the rapid dissolution of fission product phases formed during reactor irradiation, and by selective attack at zones or segregations in the fuel enriched in fission products.

The Electron Probe Micro-Analysis (EPMA) technique offers the possibility of identifying and analyzing such phases and segregations in spent LWR fuel, although the small amounts expected to be present, and the background radiation, present a significant analytical challenge.

This report describes preliminary work performed to examine the application of the EPMA technique to this problem. The fuel specimen examined had been power-bumped to a linear power rating somewhat higher than those generally experienced by commercial LWR fuel, so that fission product mobility had been enhanced. Steep concentration gradients for xenon and cesium within individual fuel grains, probably due to grain boundary sweeping during grain growth, were detected and measured. With changes in the analytical technique, it is possible that even strontium could be determined.

Godkänd av R S Forsyth

rapp\nfp8831/BEm

LIST OF CONTENTS

1 INTRODUCTION

Based on substantial experimental programmes, performed mainly in Canada, Sweden and the U.S.A. on the dissolution of spent reactor fuel in groundwaters, the current hypothesis is that the dissolution can be represented by three processes:

1. The rapid dissolution of water-soluble compounds of principally cesium and iodine which were released from the fuel matrix during reactor operation and condensed or formed reaction products in fuel cracks or in the neighbourhood of the fuel/clad gap.
2. Dissolution at preferred sites, for example, at grain boundaries.
3. Matrix dissolution.

The first process, which gives rise to the so-called "instant release fraction" of cesium and iodine nuclides within the first few days of water contact, appears to be relatively insensitive to the chemical composition of the groundwater or whether oxidizing or reducing conditions prevail. The magnitude of the "instant release fraction", not unexpectedly, has also been shown to be similar in magnitude to the release of the inert gases krypton and xenon from the fuel during reactor operation (1, 2, 3, 4).

Canadian workers later published results (5, 6) which showed that for CANDU fuel specimens exposed to a short 5-day leaching period in deionized water, only fuel which had experienced

a linear power rating higher than about 40 kW/m during irradiation gave release ratios of about unity for Cs-137 and I-129 relative to xenon release. For fuel with lower linear power ratings (25-40 kW/m), the release ratios were substantially lower, and only approached unity after 92 days leaching. This effect was attributed to retention of migrated cesium and iodine in the very small grain boundary gas bubbles, and to the limited inter-connected porosity characteristic of this fuel.

Hence, distinction between the first two of the processes listed above, "instant release" and "selective dissolution", is to a great extent a question of definition.

Nothing definite is known about the chemical state of the cesium and iodine species in the fuel which are dissolved during the first few days of water contact, or even their distribution in or on the fuel or clad for commercial LWR UO_2 fuel. Based on the numerous published reports of the outward migration of cesium and iodine observed in higher-powered fuel, it is usual to assume a location "in or near the fuel/clad gap" even for commercial fuel.

In the case of cesium, it is also postulated that the readily soluble cesium could be present as a "cesium uranate" phase, an assumption based on observations-usually qualitative and not quantitative - of such phases in high temperature fuel (7) and on Cordfunke's work on the Cs-U-O system (8) where it was shown that

$Cs_2U_4O_{12}$ could be formed near the periphery of fuel pellets.

In this context, it can be noted that for the BWR reference fuel used in the Swedish programme (Burnup: 42 MWd/kg U), about 1% of the total Cs-134 and Cs-137 inventories was released to the groundwater leachant (123 ppm bicarbonate) during the first 7 days of contact, a value in good agreement with the integral fission gas release from the whole fuel column of 0.7%.

Assuming the absence of isotopic effects, such a release corresponds to about 0.4 mg of cesium in the standard 200 ml leachant volume. Assuming, further, that the leached cesium was present in the fuel as $Cs_2U_4O_{12}$, that the phase dissolved congruently and that the dissolved uranium was retained in solution, this would give about 1.4 mg of uranium in the 200 ml leachant, a value about 7 times higher than those observed.

Experimental evidence for the second process, selective dissolution, consists mainly of leaching results reported by both Swedish and Canadian workers (9, 10, 11), which showed persistently high release fractions for cesium nuclides relative to the corresponding release fractions from uranium after contact times of several years. This appears to be the case even for the release of strontium, although here, the initial release is more than an order of magnitude lower than for cesium. For the high burnup BWR and PWR reference fuels used in the Swedish programme, the release fractions for

both cesium and strontium have been shown to be the same in both bicarbonate groundwater and deionized water (9).

Further, it has been demonstrated (1, 9) that the leaching behaviour of strontium in high burnup fuel specimens taken from different parts of the same fuel pellet column is significantly different, suggesting the effect of local irradiation history.

Clearly, a great deal of work remains to be done before an adequate understanding of these two leaching processes is attained. The problem is to a large extent an analytical problem, since the magnitude of the effects sought are extremely small and the elemental compositions to be determined represent a severe test of the sensitivity and accuracy of available investigational techniques.

The detailed characterization of spent fuel before and after its exposure to groundwater is an important part of the Swedish programme. This report presents the results of SEM/EPMA examination of a spent fuel specimen performed with the aim of method development. The fuel specimen selected for examination had a burnup (37 MWd/kg U) somewhat lower than the reference BWR and PWR rods, but had been subjected to a power bump test in Studsvik's R2 test reactor. The local maximum power which the specimen had experienced was 43 kW/m, so that fission product mobility was expected to be appreciably higher than in typical LWR fuels.

2 EXPERIMENTAL

A thin diametral strip was cut out from a metallography specimen prepared from a BWR fuel rod with a burnup of approximately 37 MWd/kg U, which had been subjected to a staircase ramp terminating at a local linear heat rating of approximately 43 kW/m, with a hold time of 12 hours. The surface was ground and polished in a non-aqueous medium, with 0.05 μm alumina as the final stage.

The uncoated specimen was mounted in a holder together with the X-ray standards. The EPMA was performed on a JEOL JXA-840 analytical SEM, equipped with two wavelength dispersive X-ray spectrometers, partly shielded with lead. The analysis was controlled by a LINK AN10000 X-ray microanalysis system, with stage and beam automation.

The analysis was performed with a beam current of 300 nA at an accelerating voltage of 20 kV, in order to give a reasonable peak-to-background ratio for the active specimen. The electron beam current, peak and background heights were measured on the standards prior to each measurement series, or after any change in the instrument operating conditions. The standards and X-ray lines are shown in Table 1. In the case of Xe and Cs, pseudo-standards were used, since suitable analysis standards for these elements were not available.

After the standardization, the stage was driven to the specimen position, beam points for analysis were programmed, and a digital secondary electron image was stored with the analysis points. The peak and background heights were then measured for each element at each point, together with the beam current. After the measurement series was complete (usually about 30-60 minutes), the image was recorded again, in order to check for any drift due to heating or charging.

The results were then corrected for changes in beam current (≤1%) and a ZAF correction was calculated (for the listed elements).

Table 1 EPMA standards and X-ray lines

Element	Standard	Line	Crystal
Sr	SrF_2	$L\alpha_1$	TAP
Xe	Te*	$L\alpha_1$	PET
Cs	BaF_2*	$L\alpha_1$	PET
Nd	NdF_3	$L\alpha_1$	PET
U	UO_2	$M\alpha_1$	PET

3 ANALYSIS

The measured concentration for each fission product (atom %) was normalized to the measured concentration of uranium, in order to avoid any effect of local porosity. In the discussion below, all the concentrations refer to atom % excluding oxygen (i.e. assuming there is no oxygen). There were, however, many other non-negligible sources of error, some of which will be briefly discussed here.

3.1 Specimen activity

The specimen activity contributes greatly to the background intensity, despite the partial shielding of the spectrometers. In order to reduce this background, a relatively narrow voltage window was used in the pulse height analyser. This could have decreased the accuracy somewhat when dealing with variable count rates.

Since the standards were measured with the active specimen present, no other corrections were made to deal with the specimen-induced background. The activity background intensity varied by up to a factor two between the different elements, and with the specimen position. The activity background intensity was similar for both the specimen and the standards, and in all cases the peak-background count rate was approximately zero.

3.2 Standards

When using standards for quantitative EPMA, the measurement on the standards can also be a source of error. Two of the major problems encountered here were the lack of suitable standards for Xe and Cs, and inhomogeneity/porosity in the ceramic standards. Te and Ba were used as pseudo-standards for Xe and Cs respectively, and the relative line intensities of the pseudo-standards to the elements were estimated by extrapolation from other nearby elements. Inhomogeneity/porosity related spread in the measured intensity was most marked for the UO_2 and NdF_3 standards. This effect was not corrected for in this study.

A special problem was encountered with the Sr standards, where the background intensity was very high and variable. This was probably due to an inappropriate choice of wavelength used for the background measurements, in an attempt to avoid possible overlapping with other elements present in the specimen.

3.3 Overlapping lines

In addition to U and O, a high burnup fuel specimen also contains small amounts of a large number of fission and neutron capture products. These elements have X-ray lines which may overlap with the analysed elements' lines, or affect the background intensity measured on either side of the analysed lines. An example of this is a number of U lines in the vicinity

of the Cs $L\alpha_1$ line. Despite the use of a pulse height analyser to filter out higher order reflections of higher energy X-rays, a scan on the UO_2 standard showed substantial variations in the measured intensity in the vicinity of the Cs line. It was possible, however, to choose wavelengths for the background measurements which gave the correct " background" intensity on UO_2 at the $CsL\alpha_1$ line wavelength.

For Nd, the peak-background intensity measured on the UO_2 standard gave a calculated Nd concentration of about -0.08 atom %, i.e. the Nd concentrations measured on the specimen were probably 0.08 atom % too low. This problem was not encountered with the other analysed elements.

3.4 ZAF correction

The AN10000 performed a full ZAF correction for the elements analysed. However, the fission and neutron capture products not analysed (about 5 atom % in total), as well as oxygen, were not included in the correction. This is not a significant source of error.

3.5 Minimum detectable concentration

The sensitivity of concentration determinations can be expressed in terms of the minimum detectable concentration, i.e. the smallest concentration detectable at the 2σ level. The sensitivity can thus be expressed as

$$(P-B) \geq 2\ (\sigma_P^2 + \sigma_B^2)^{\frac{1}{2}}$$

where P and B are the peak and background intensities (heights), and

σ_P and σ_B are the standard deviations of the spread in the intensities.

The standard deviations of the background intensities were determined from the measurements on the specimen. Similarly, the standard deviation of the peak intensity for Nd was estimated from the measurements, since Nd is immobile, and has a relatively constant fission yield over the area investigated. For the other elements the standard deviation of the peak intensity was assumed to be the square root of the peak count.

The estimated minimum detectable concentration for each analysed element is given in Table 2, for the typical levels found in the specimen. For Sr, the minimum detectable concentration is seen to be far larger than the typical amounts measured in the specimen, while for the other fission products the sensitivity is of the order of 10% of the measured concentrations.

3.6 Accuracy

The overall accuracy of the measurements is difficult to ascertain without comparison or benchmarking with other, more accurate, analysis methods. However, a rough guide to the relative accuracy can be estimated from the identified error sources. The estimated total error, relative to the mean measured concentra-

tion of each element, is given in Table 2. Since the total error contains both systematic and random errors, some of which are independent of the actual element concentration in the specimen, the relative error is larger for lower concentrations and smaller for higher concentrations than the mean. The random errors (such as the minimum detectable concentration described in point 3.5 above) are the measured or estimated 1σ values (where applicable).

The total error in the Nd measurements can be halved by correcting for the U line overlap effect (see point 3.3). An improvement in the relative accuracy of both Nd and U could also be attained relatively easily by "fixing" the value of the peak-background intensity to estimate the scatter due to porosity or inhomogenity in the standards.

Table 2 Detection sensitivity and estimated overall accuracy

Element	Min. MDC detectable conc. Atom %	Relative accuracy %
Sr	1.0	300
Xe	0.1	6
Cs	0.05	10
Nd	0.07	20
U	0.3	4

3.7 Spatial resolution

The spatial resolution of the X-ray analysis is determined to a large extent by the source size of the X-rays. This in turn is determined by the volume of the specimen material in which the characteristic X-rays are generated. Other factors affecting the resolution are secondary fluorescence (i.e. characteristic X-rays generated by other X-rays), drift in the electron beam or specimen position, and local variations in density (pores or cracks).

For the instrument conditions used in this study, the effective X-ray source size for the analysed lines has been estimated to be approximately 0.6 µm in diameter (12). This assumes a point electron beam, and no secondary fluorescence.

The "qualitative" resolution (i.e. ability to detect well-defined areas of different composition) can also be estimated with the formula (13):

$$d = 7.7 \times 10^{-2} \frac{1}{\rho} (E_o^{1.5} - E_c^{1.5})$$

where d is the resolution in µm
ρ is the specimen density in g/cm^3
E_o is the accelerating voltage in kV
E_c is the critical excitation potential of the X-ray line in kV

This formula also gives a value of about 0.5-0.6 µm. However, the electron beam diameter was of a similar size, so that the resolution

was approximately 0.8 µm. Belk (14) considers that the attainable resolution for quantitative analysis is about 3-4 times poorer (i.e. approximately 3 µm).

There is a secondary fluorescence contribution to the $SrL\alpha_1$ line due to excitation by the UMα emission, as well as an effect on all the analysed lines due to excitation by the UL and continuum X-rays. The total secondary fluorescence effect on the resolution is difficult to quantify, but is not considered a major limitation to the resolution.

The drift in the position of the electron beam relative to the specimen was checked by comparing the image acquired prior to the analyses with the image acquired afterwards. In most cases there was some observable drift, sometimes as much as 5 µm. The drift was probably due to specimen heating and charging, and varied according to the location (more drift near to cracks or the edge of the specimen) and time.

The effect of local changes in the density due to cracks or pores is difficult to assess. Large pores and cracks could be expected to significantly increase the X-ray source volume, possibly affecting the resolution by a factor of two.

The depth resolution (i.e the depth from which the X-ray emissions emanate) was probably less than 1 µm in all cases apart from close to cracks or large pores.

4 RESULTS AND DISCUSSION

A photomacrograph of a longitudinal section of a portion of the power-bumped rod is presented in Fig 1, which also shows the location of the thin, 1.5 mm wide fuel section removed from a mid-pellet position for the measurements described in this report. Fig. 2 presents a series of photomicrographs showing the fuel structure in the as-polished condition from the fuel pellet centre out to near the pellet periphery.

The fuel rod had experienced appreciable release of the fission gases Kr and Xe, and redistribution of cesium out towards the pellet periphery (demonstrated by micro-gamma scanning) during the power bump, and this is reflected in the radial variation in structure and, particularly, the amount and morphology of the porosity. Spherical or near-spherical metallic inclusions of the fission product metals Mo, Tc, Ru, Rh and Pd are also seen to be present out to over half the pellet radius.

At the peak power position in the rod, where the ramp maximum linear power was substantially higher than 43 kW/m, ceramographic examination after etching (results not presented here), showed the presence of populations of small pores within the fuel grains, and also areas free of such pores. These zones were interpreted as areas swept by the grain boundaries during grain growth, and such effects were also anticipated in the central parts of the specimen examined in this work. The specimen used for the SEM/EPMA examination was, of course,

unetched to avoid fission product loss,so the internal grain structures are not so clearly visible.

Since the principal aim of this work was to assess the possibility of detection and measurement by the EPMA technique of possible concentration gradients in individual fuel grains and at crack surfaces with particular attention to cesium and strontium, this specimen was regarded as being particularly suitable.

At a series of radial positions, point scans have been performed covering individual grains, grain boundaries and areas of porosity in order to detect and measure possible local concentration gradients. Steps of 1-3 µm were used to be able to assess the effective spatial resolution. Inspection of Fig. 10b indicates that the measured resolution was in good agreement with the theoretical value (section 3.7).

Two locations near a fuel crack surface at a radial position of 2.5 mm, where fuel reaction with cesium released from the hotter central portions of the fuel pellet was possible, were also examined.

Only 5 elements were determined at each position:

1. **Uranium**
   The measured atomic percentages of the other 4 elements are reported in the following as ratios to uranium.

2. **Neodymium**
   This element is regarded as being immobile within the UO_2 lattice and

its concentration is roughly proportional to the local burnup. (Nd-148 is the usual monitor of burnup.)

3. **Cesium**

4. **Strontium**

5. **Xenon**

The results for the measurements on individual grains are presented in Figs. 3-12 as paired SEM photographs and concentration profiles. The positions of the individual measurement points are indicated as crosses in digital image photographs with arbitrarily arranged grey scales which are also provided to facilitate comparison.

Fig. 13 is a SEM photograph of the fuel crack at a radius of 2.5 mm showing the two locations which were examined for possible Cs-UO_2 reaction zones. Fig. 14 presents the results for location 1, a large fuel grain separated from the fuel matrix by a micro-crack, suggesting the possibility of grain boundary separation due to weak crack bonding. Fig. 15 shows location 2, where the presence of secondary phases was suspected.

The burnup of the fuel examined was calculated to be about 37 MWd/kg U from reactor operation data, a value sufficiently accurate for our purposes in this work. Using ORIGEN-2, the atomic ratios of the 4 fission products measured relative to uranium were calculated to be:

Xe; 1.1% Cs; 0.55% Sr; 0.25% Nd; 0.76%

These values, of course, refer to the bulk fuel and take no account of the enhanced burnup at the fuel pellet rim or the radial burnup gradient.

The Nd/U atomic ratios plotted in Figs. 3-15 exhibit satisfactory precision (i.e., reproducibility) but lie at values between 0.4 and 0.5%. Even allowing for the negative bias reported in section 3.3, this seems somewhat low. This will be investigated in future work on more typical LWR fuels when a more thorough characterization of the fission product inventories will be performed.

The Sr/U ratios also appear to be low (0.1-0.2%), but as discussed earlier, the minimum detectable concentration associated with the background subtraction method used in this preliminary work was substantially larger than the specimen levels. Hopefully this can be improved upon in later work.

Xenon and cesium are fission products which are released from the central parts of the pellet, to the free internal rod volume in the case of xenon, and to the cooler outer fuel annulus and the clad in the case of cesium. Further, as is demonstrated in this work, the grain boundary sweeping process produces steep local concentration gradients within individual grains which leaves small fuel zones with Xe/U and Cs/U ratios approaching the bulk inventory values even at radial positions where general depletion has occurred.

It must be remembered that the positions in the fuel selected for the measurement scans were specifically located to areas where such gradients could exist, and are not representative of the bulk fuel behaviour at the same radial position.

However, the xenon and cesium concentration profiles shown in Figs. 3-12 illustrate the general trend for xenon release and cesium redistribution in addition to local effects. At a radial position 1 mm from the fuel centre (Figs. 3 and 4), almost total depletion of both elements is observed, while at 2 mm and 2.5 mm (Figs. 5-10) the Xe/U ratio is either zero at grain boundaries and swept areas or approaches the ORIGEN-2 value. The Cs/U ratio shows the same spatial variation as the Xe/U ratio but the maximum concentrations are still significantly lower than the calculated inventory level.

At 3 mm from the fuel centre (Figs. 11 and 12) the Cs/U ratio has attained the general level of the ORIGEN-2 value but the concentration profiles also show pronounced maxima, probably associated with grain boundary porosity. At this position, the Cs and Xe concentration profiles are very dissimilar, with poor correlation between the positions of the maxima. It is therefore inferred that the "matrix" cesium level represents un-redistributed cesium, while the cesium maxima represent cesium from the hotter portions of the fuel.

In the case of the measurements performed at and near the fuel crack at a radial position of

2.5 mm, the fission product/uranium ratios are presented as concentration maps. (Figs. 14 and 15). Here, the comments above with respect to the Nd/U and Sr/U ratios also apply. The Xe ratio also shows the same steep concentration gradients associated with grain boundary sweeping as was observed in the fuel pellet matrix.

The cesium results, however, show significant differences compared with the previous scans. Firstly, the general level of the concentration profiles are as high or higher than the level observed at a radial position of 3 mm in the fuel pellet matrix. The ratio value of 0.48% measured a few microns into the matrix from the micro-crack (Fig.14b), gives some support to the hypothesis that the cesium "enrichment" observed is due to transport along the crack.

Secondly, at each location, one measurement made with the beam overlapping the fuel/crack edge gave a Cs/U ratio higher than 3%. This may, of course, be a consequence of a step change in the level of background correction, as is almost certainly the case for the strontium results at the same positions.

5 CONCLUSIONS

The application of the electron probe microanalysis technique to the examination of a spent fuel specimen at the individual grain level has shown that the technique has the capacity to distinguish and measure fairly small compositional changes over short (1-2 microns) distances with satisfactory sensitivity and accuracy for the fission products xenon, cesium and neodymium. With some changes in the measurement technique, further improvements in accuracy can be attained, and it is possible that even strontium could be measured with sufficient accuracy to enable significant concentration changes to be detected.

In the fuel specimen examined, which had experienced a power ramp up to 43 kW/m such that appreciable fuel restructuring and fission product migration and release had occurred, steep local concentration gradients probably associated with grain boundary sweeping were detected and measured. An enhanced cesium/uranium ratio in fuel grains at a crack position was tentatively detected.

Application of the technique to the examination of high burnup commercial LWR spent fuel specimens is planned for the near future. Later, specimens which have been exposed to leaching will also be examined.

REFERENCES

1. U-B EKLUND and R.S. FORSYTH, SKB Technical Report 70, Stockholm, Sweden (1978).

2. R.S. FORSYTH. K SVANBERG and L.O. WERME, in Scientific Basis for Nuclear Waste Management VII, edited by G.L. McVay (Elsevier Science Publishers, New York, 1984) p 179.

3. R.S. FORSYTH and L.O. WERME, SKB Technical Report 87-16, Stockholm, Sweden (1987).

4. L.H. JOHNSON, K.I. BURNS, H.H. JOHRIG and C.J. MOORE, Nucl. Technol., 63, 470 (1983).

5. L.H. JOHNSON et al., Proc. Topical Mtg. Fission Product Behaviour and Source Term Research, Snowbird, Utah, July 15-19, 1984, p 15, American Nuclear Society (1985).

6. S. STROESS-GASCOYNE, L.H. JOHNSON and D.M. SELLINGER, Nucl. Technol., 77, 320 (1987).

7. H. KLEYKAMP, J. Nucl. Mater. 131 (1985) 221.

8. E.H.P. CORDFUNKE, Proceedings, Symposium on Thermodynamics of Nuclear Materials, Vienna, Oct. (1974): IAEA-SM190/6.

9. R.S. FORSYTH, L.O. WERME and J. BRUNO, J. Nucl. Mater. 138, 1 (1986).

10. L.O.WERME and R.S. FORSYTH in Scientific Basis for Nuclear Waste Management XI, edited by M.J. Apted and R.E. Westerman Material Research Society, Vol 112 p 443 (1987).

11. L.H. JOHNSON, D.W. SHOESMITH and S. STROESS-GASCOYNE in Scientific Basis for Nuclear Waste Management XI, edited by M.J. Apted and R.E. Westerman. Materials Research Society, Vol 112, p.99 (1987).

12. L.S. BIRKS, "Electron probe microanalysis", Wiley-Interscience, New York (1971).

13. S.J.B. REED, in "X-ray optics and microanalysis" (R. Castaing et al., eds.), Hermann, Paris (1966).

14. J.A. BELK, in "Quantitative scanning electron microscopy" (D.B. Holt et al., eds.), Academy Press, London (1974).

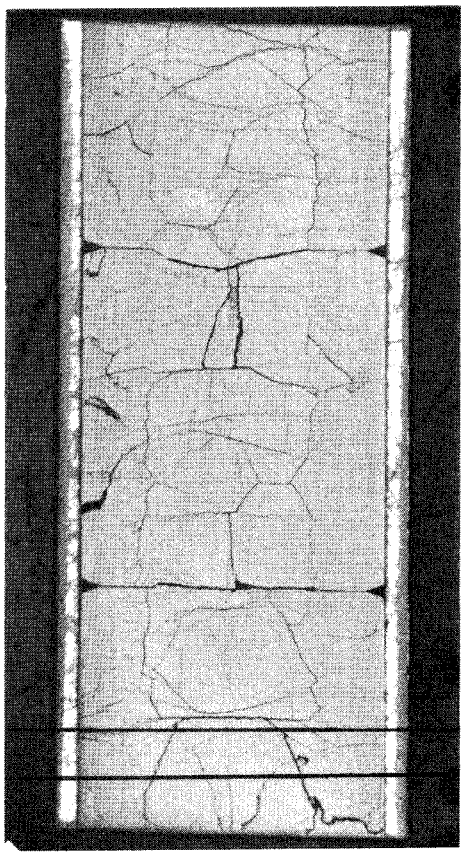

SPECIMEN 1313A

1.5 mm

Fig 1. Photomacrograph (x4) showing location of the fuel specimen used for ceramographic and SEM/EPMA examinations.

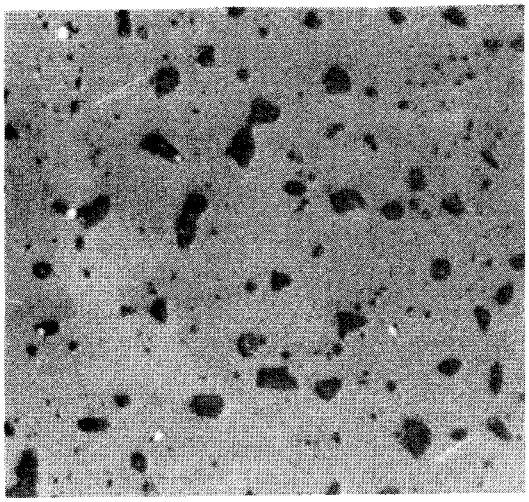

Centre

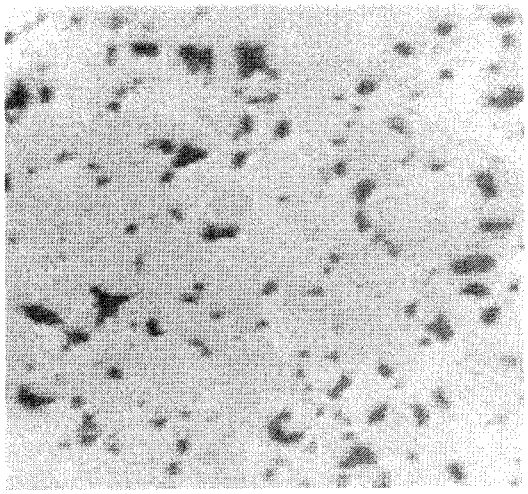

r = 2.5 mm

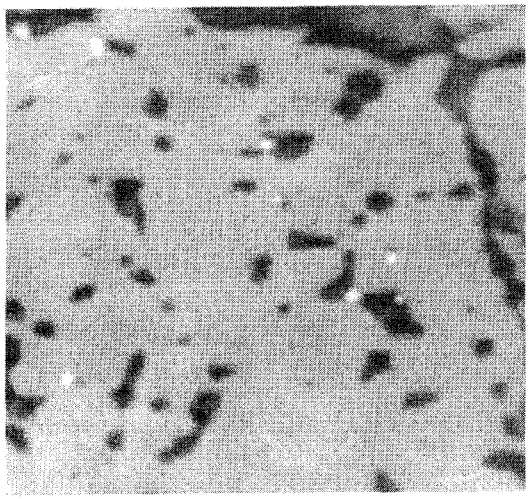

r = 1 mm

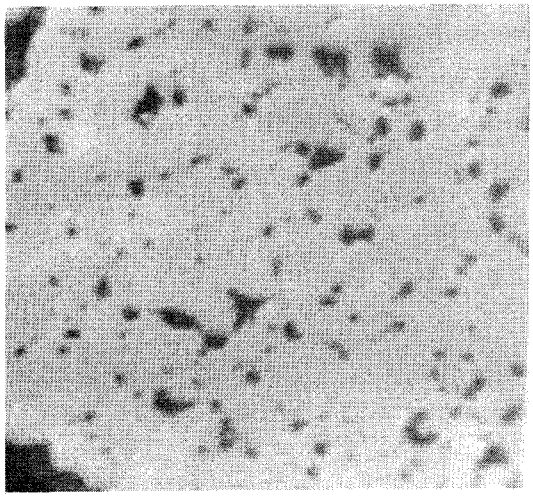

r = 3 mm

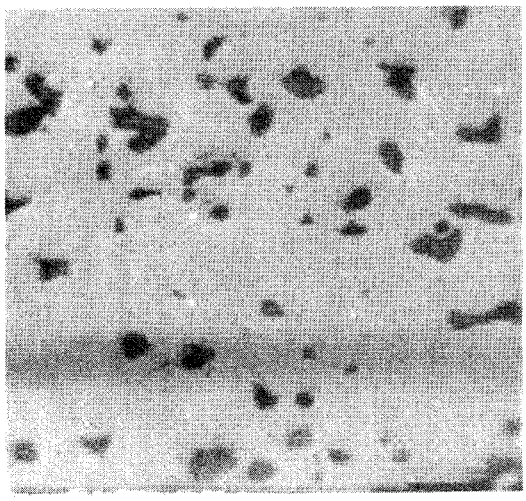

r = 2 mm

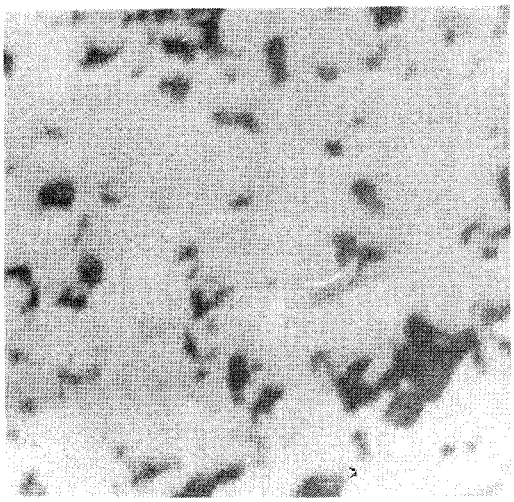

r = 5 mm

Fig 2. Photomicrographs (x1000) of the fuel as polished.

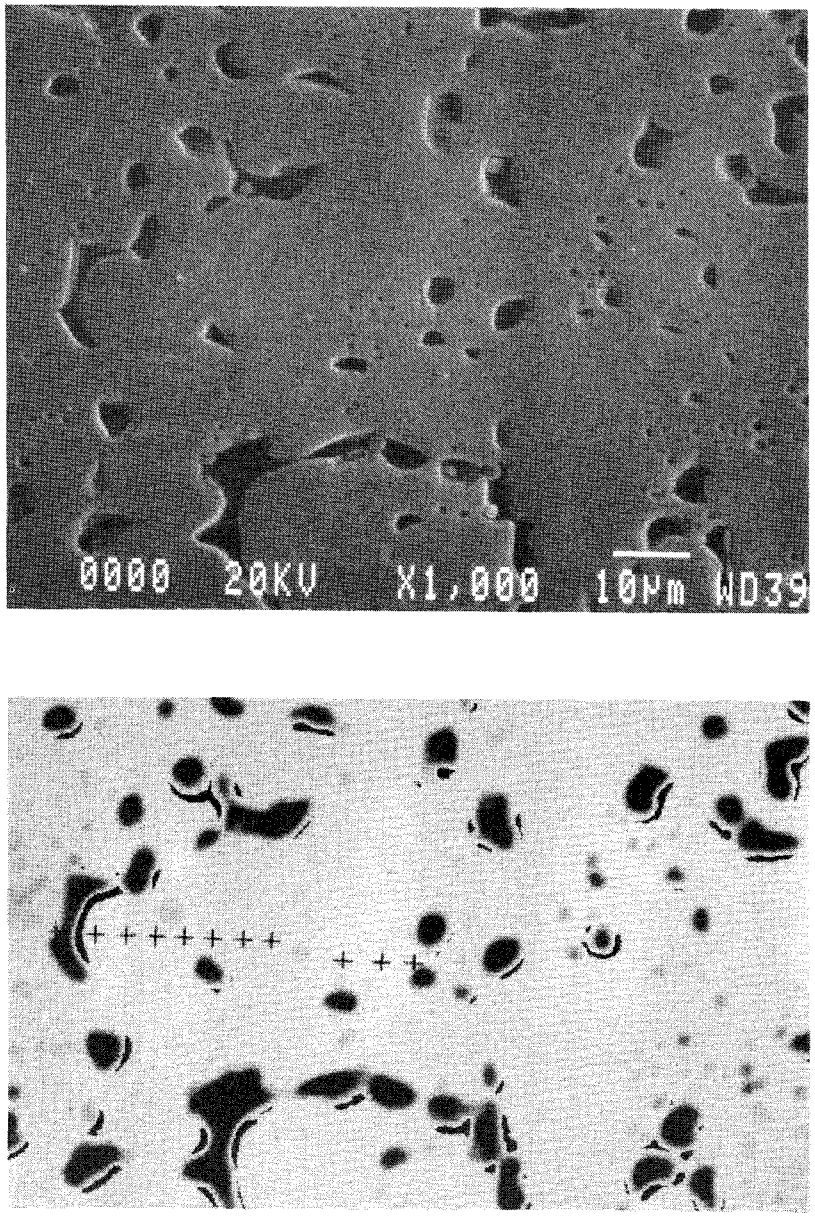

Fig 3a. 1 mm from fuel centre.
Scan A

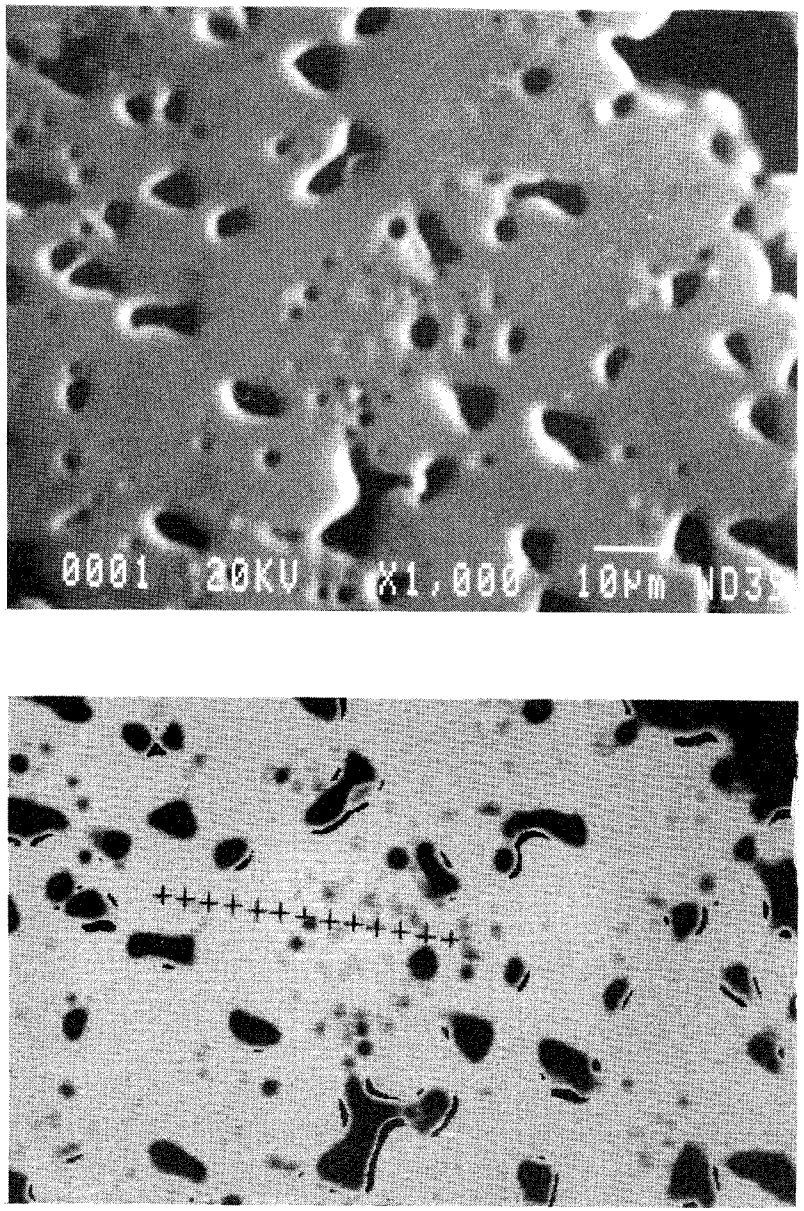

Fig 4a. 1 mm from fuel centre.
Scan B

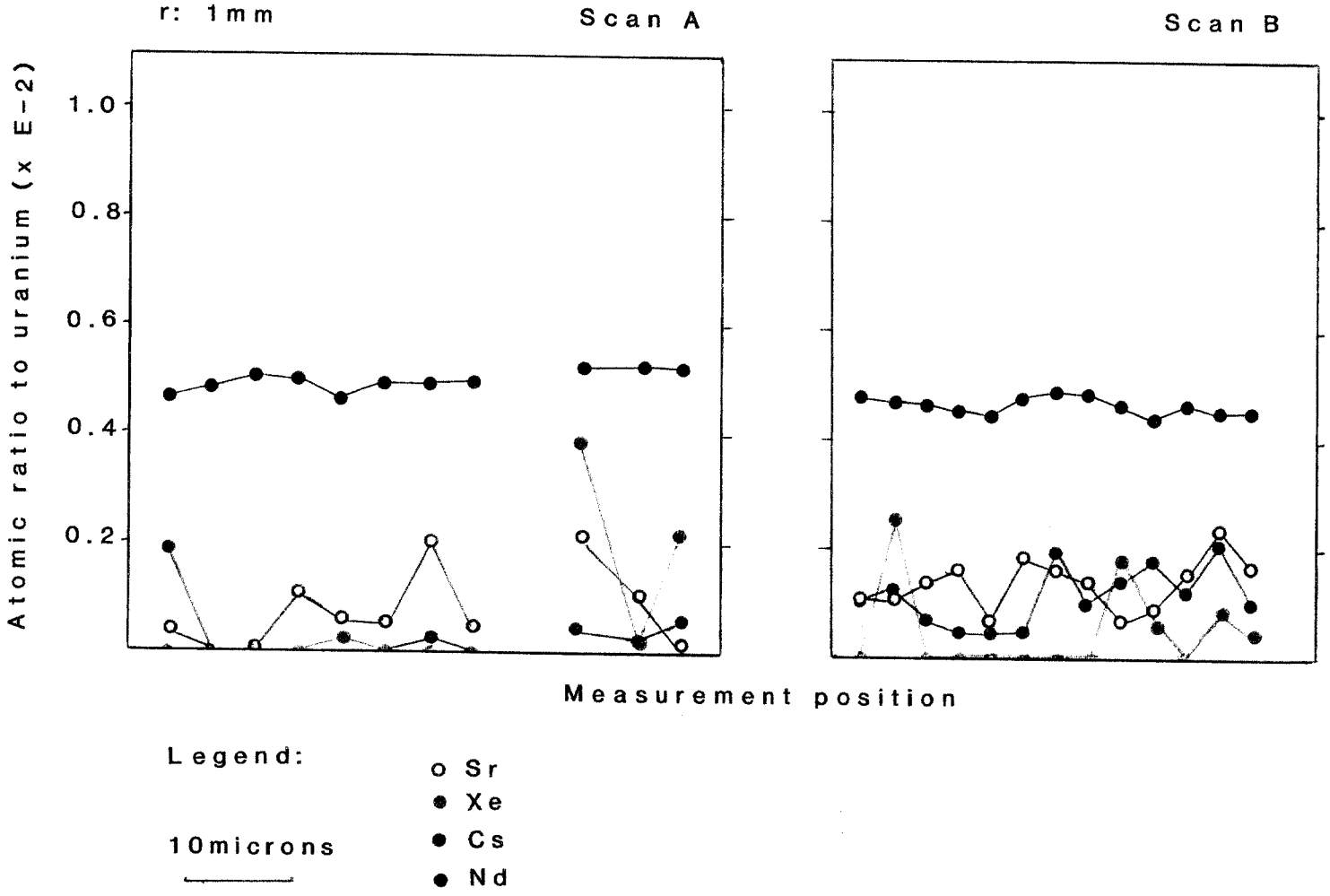

Figs 3/4b. Concentration profiles.
(See Figs. 3a and 3b)

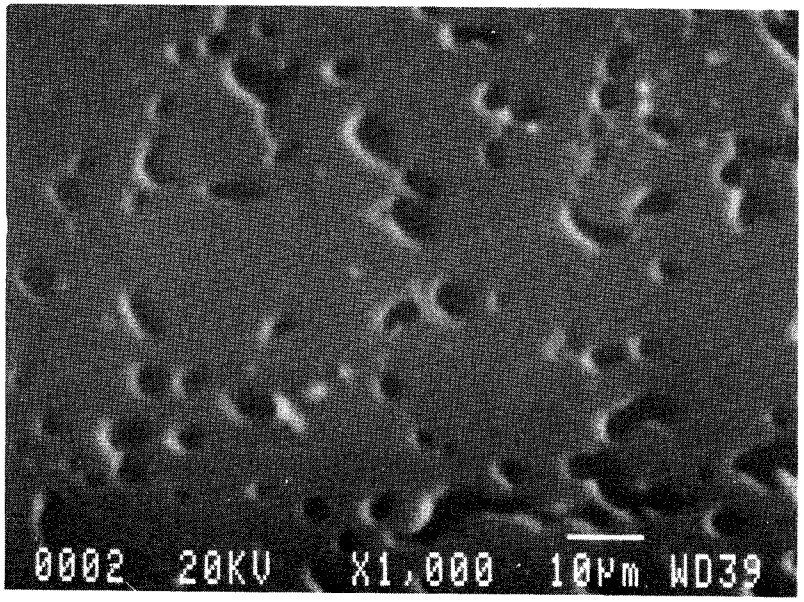

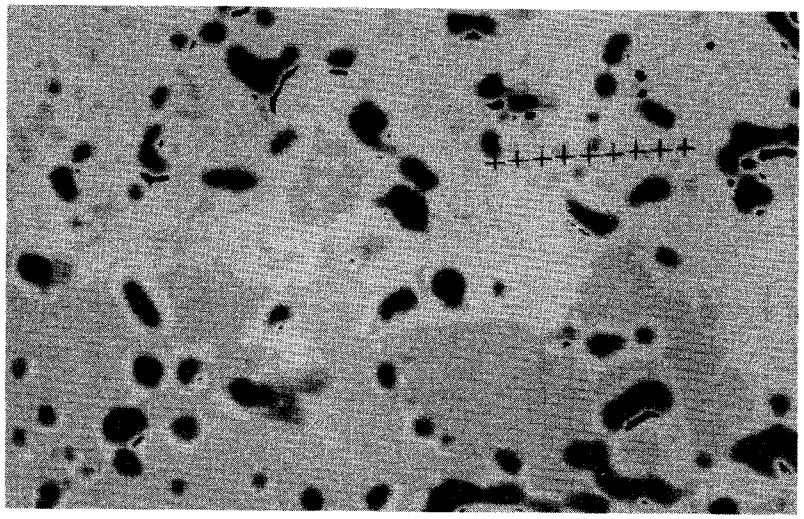

Fig 5a. 2 mm from fuel centre.
Scan A

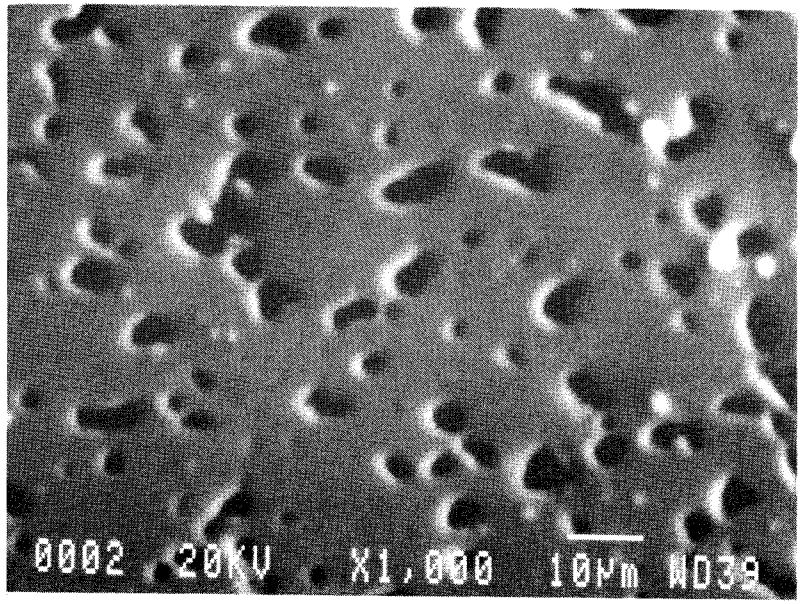

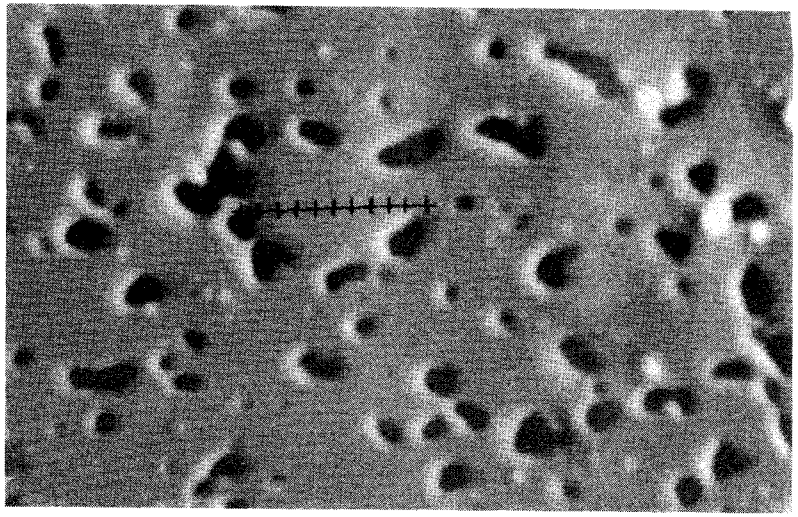

Fig 6a. 2 mm from fuel centre.
Scan B

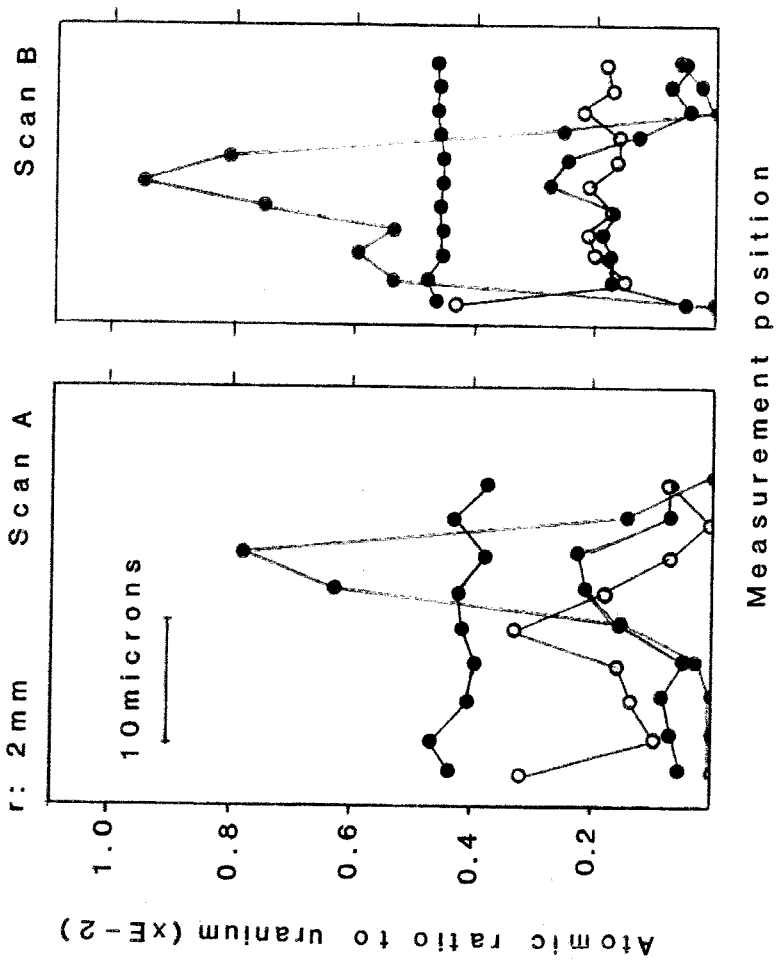

Figs 5/6b. Concentration profiles.
(See Figs. 5/6a)

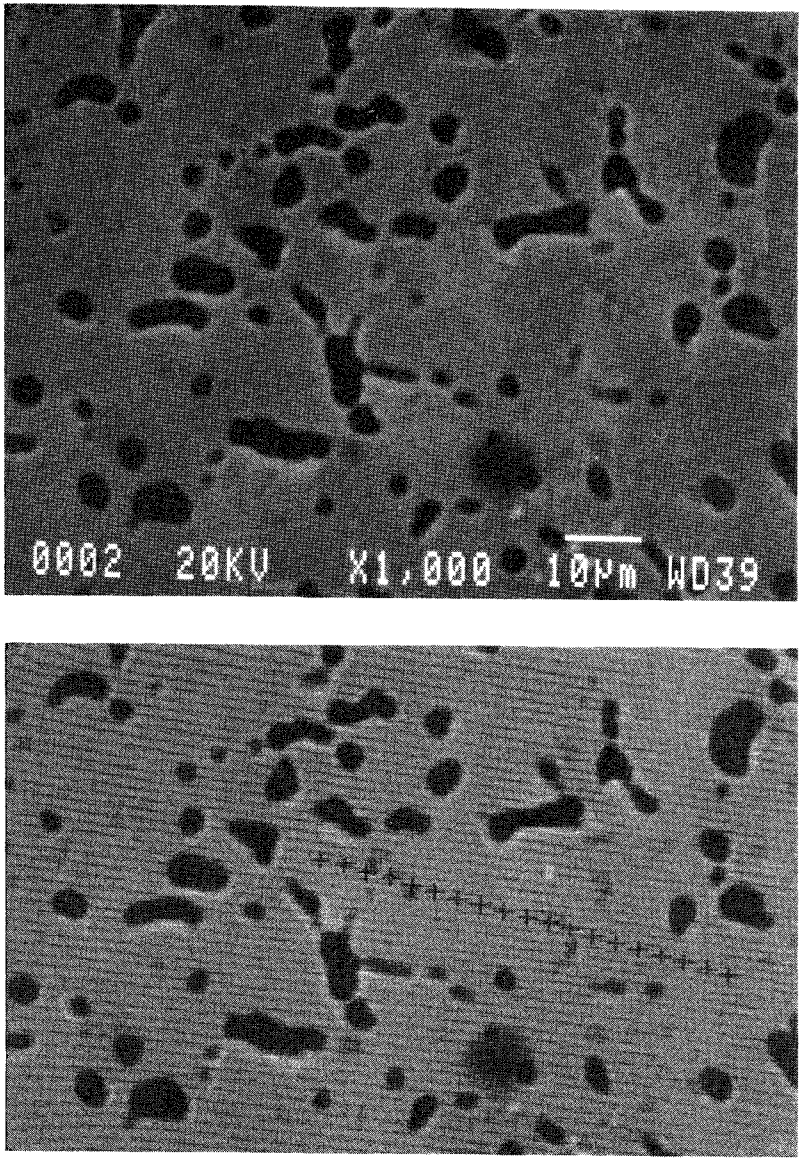

Fig 7a. 2 mm from fuel centre.
Scan C.

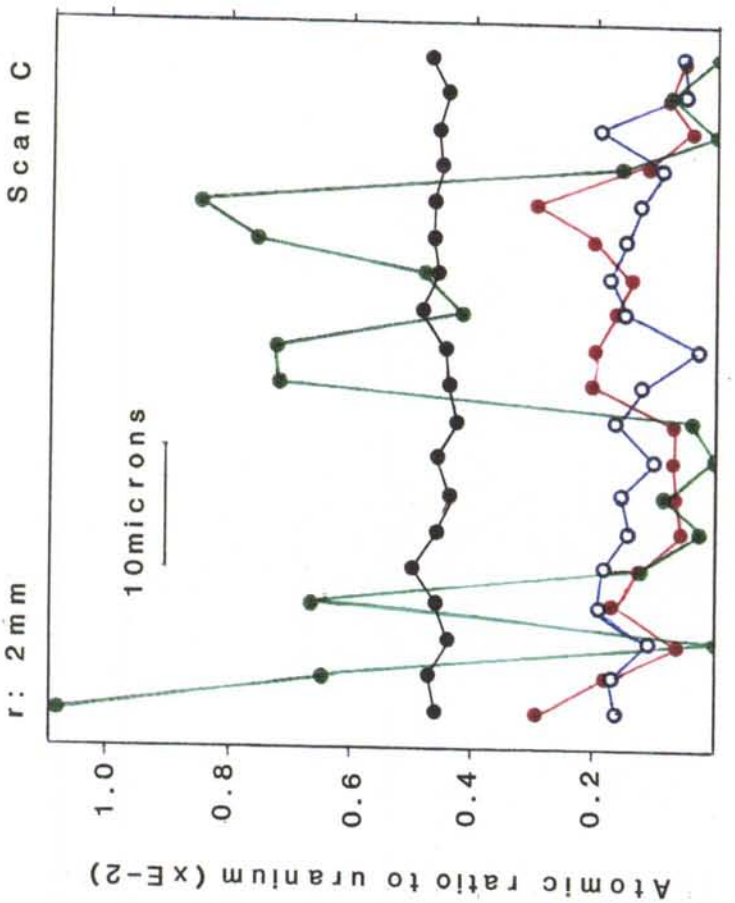

Fig 7b. Concentration profiles.
(See Fig 7a)

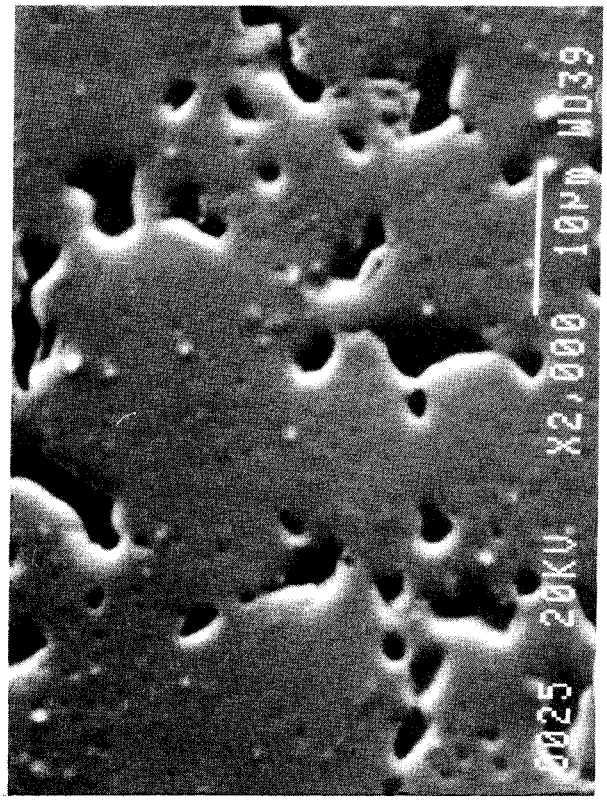

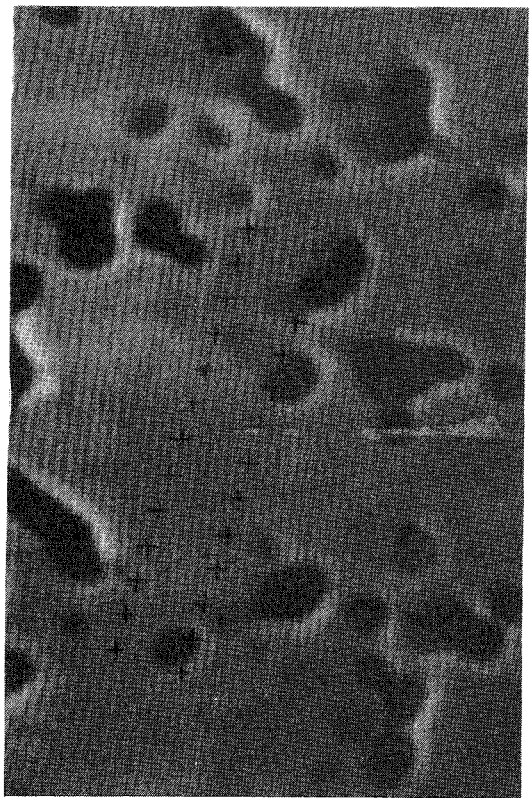

Fig 8a. 2.5 mm from fuel centre.
Scan A.

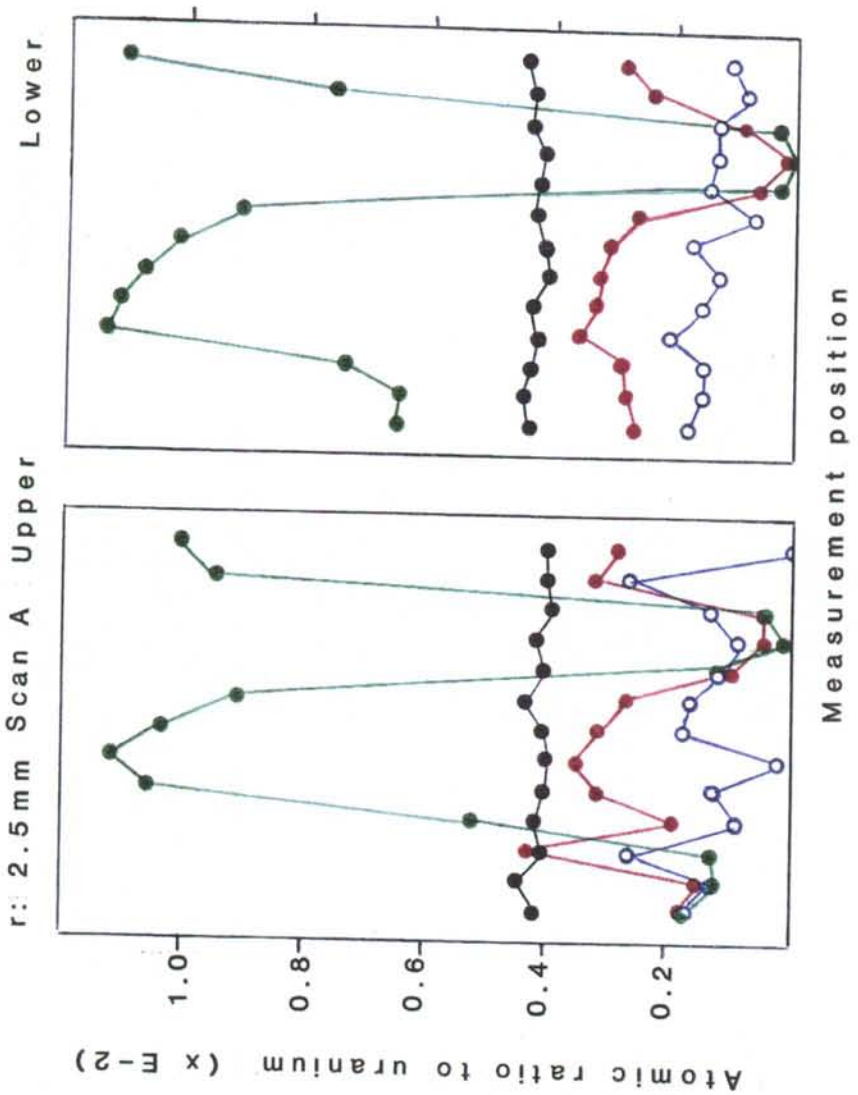

Fig 8b. Concentration profiles.
(See Fig 8a)

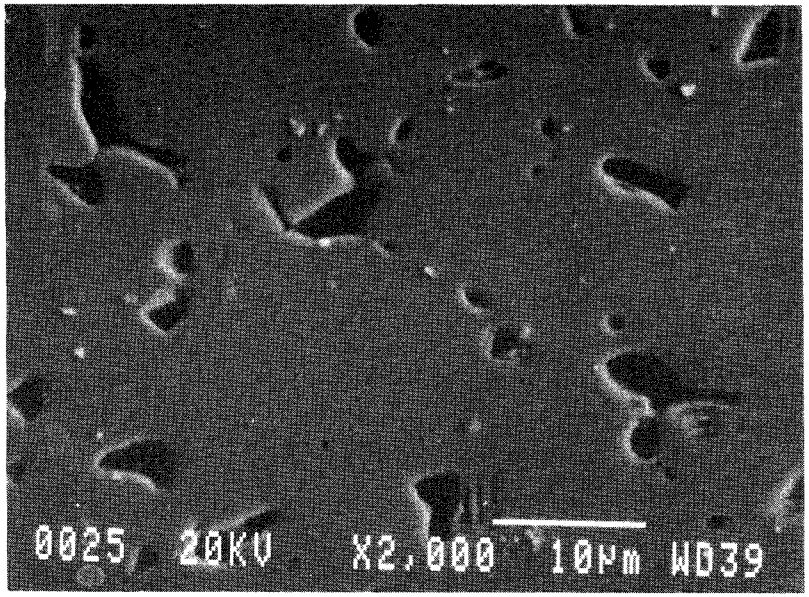

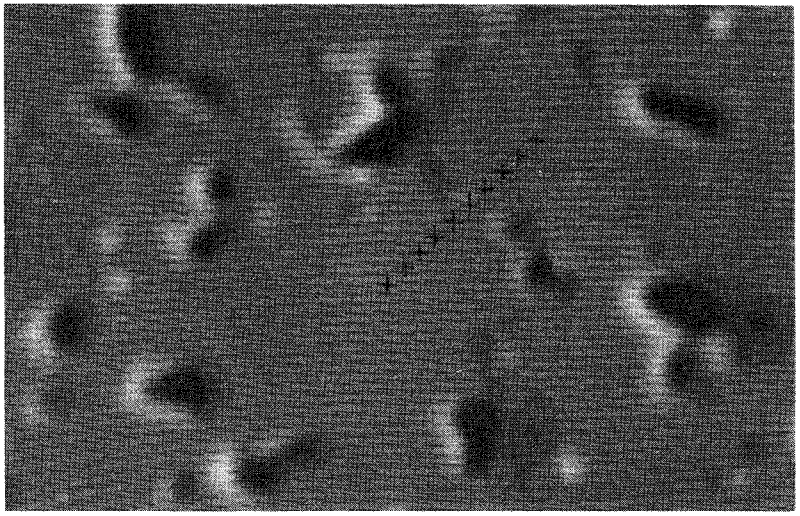

Fig 9a. 2.5 mm from fuel centre.
Scan B

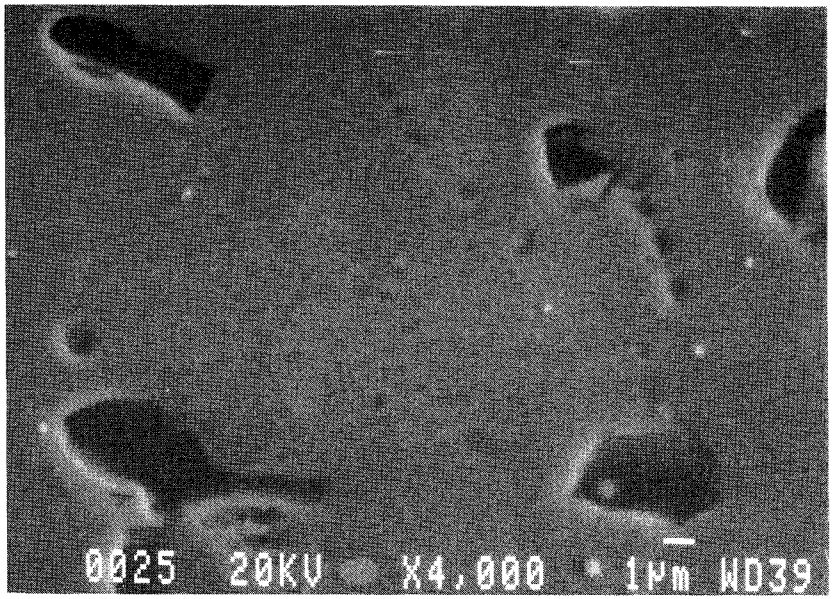

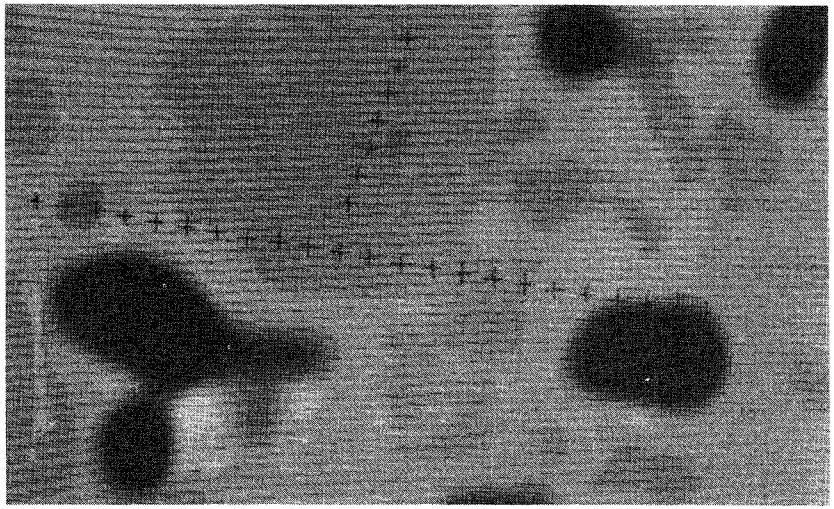

Fig 10a. 2.5 mm from fuel centre.
Scan C

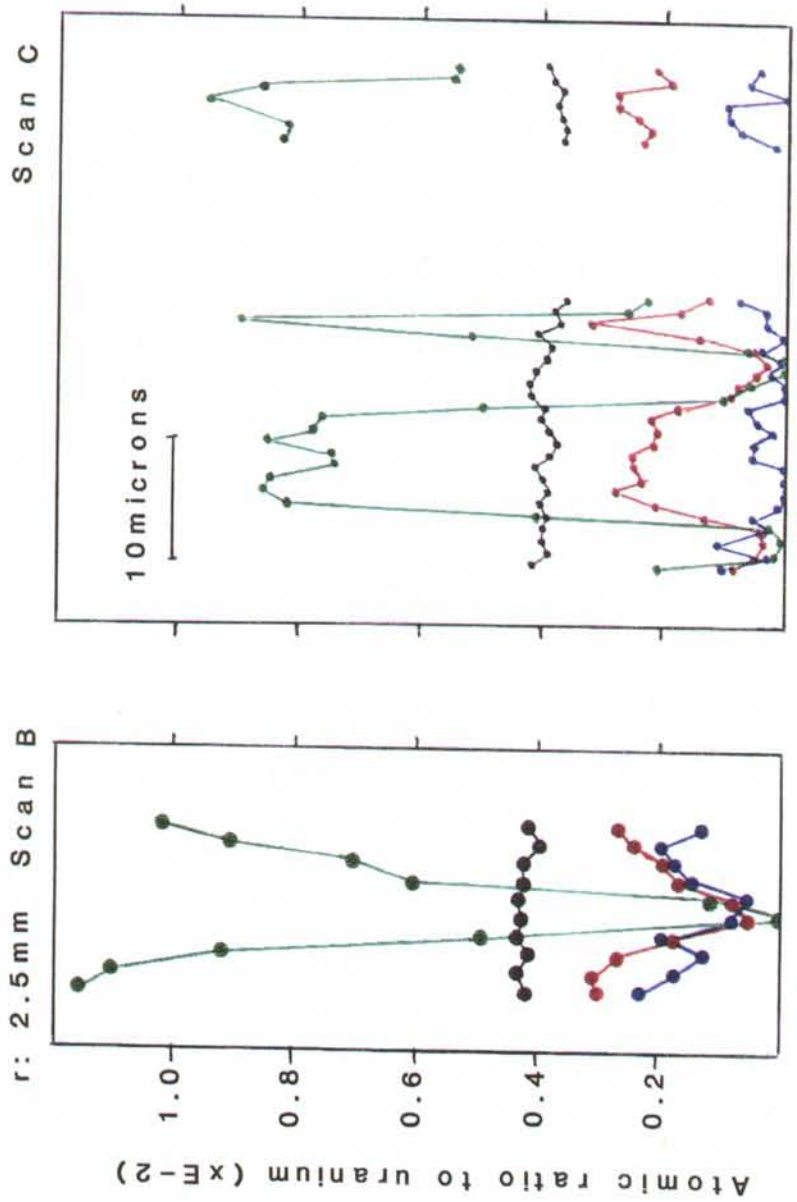

Figs 9/10b. Concentration profiles.
(See Figs 9/10a)

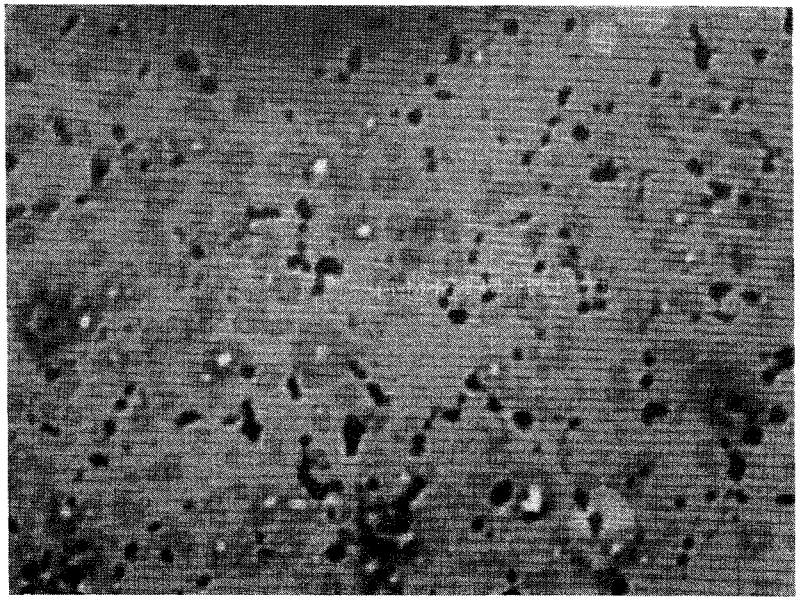

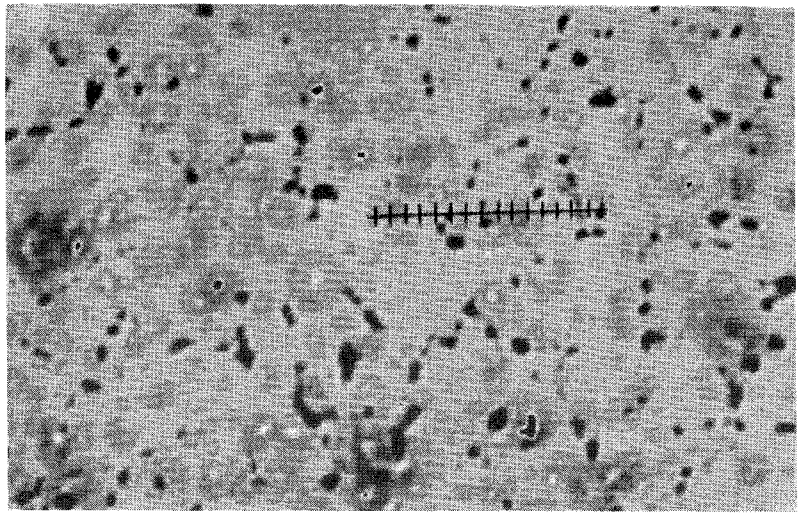

Fig 11a. 3 mm from fuel centre.
Scan A

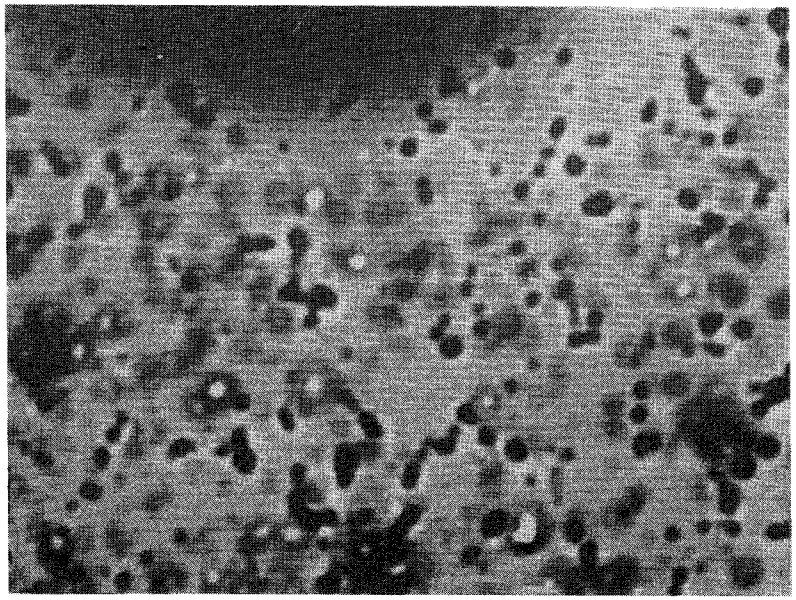

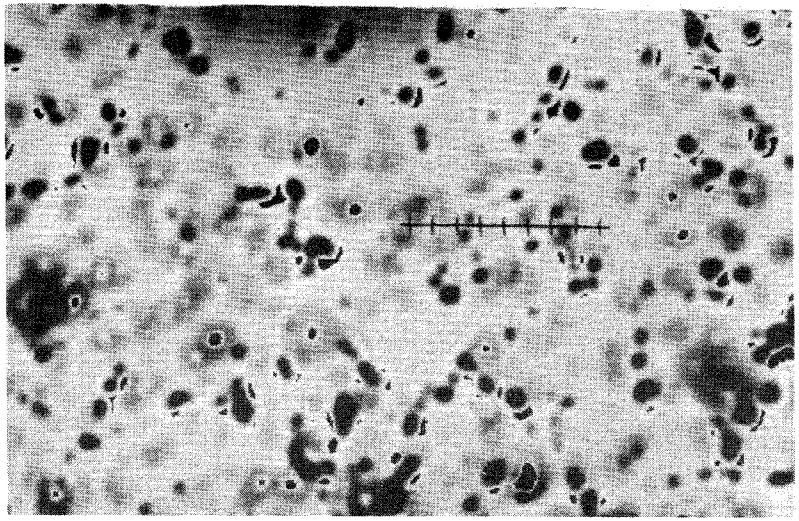

Fig 12a. 3 mm from fuel centre.
Scan B

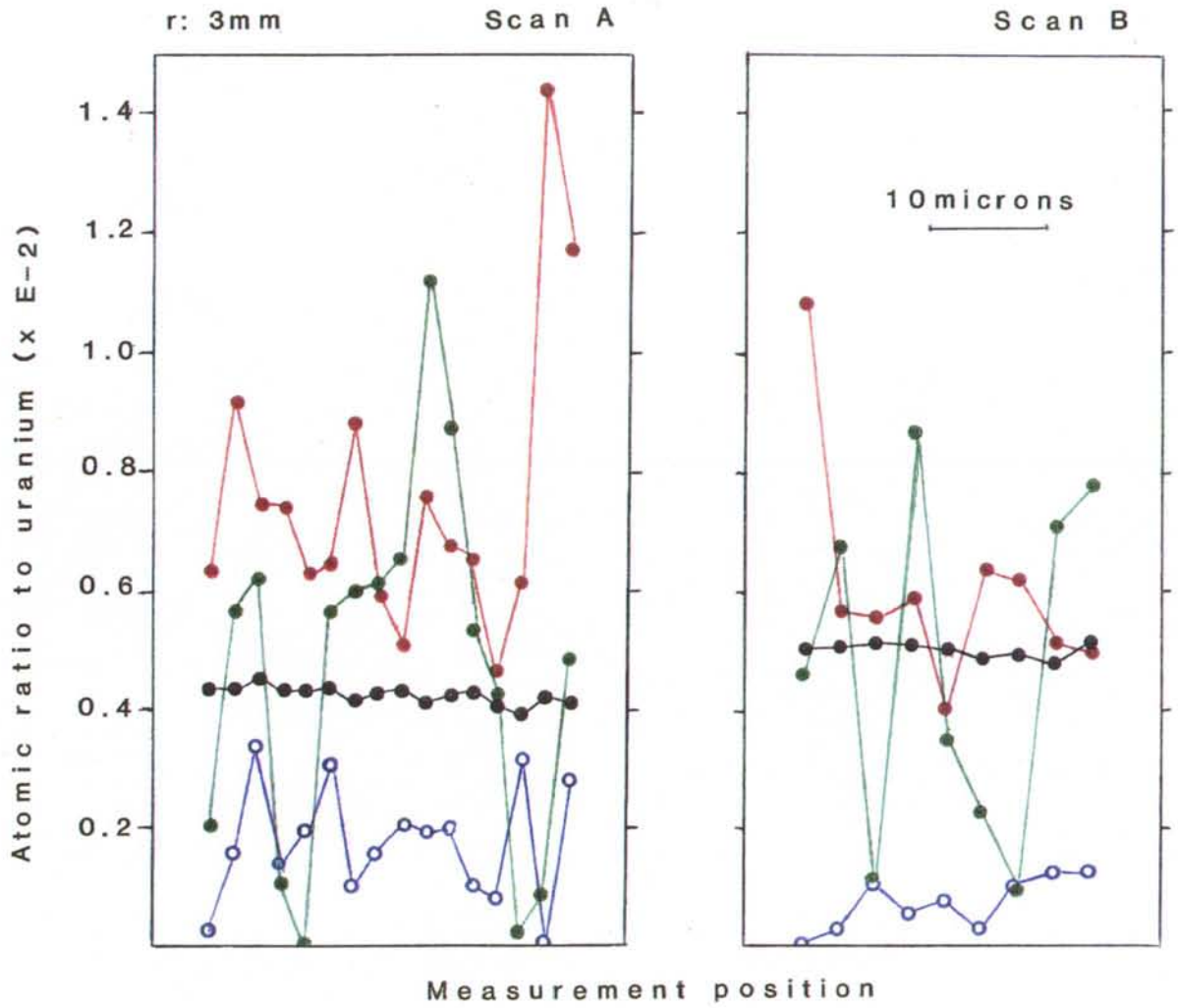

Figs 11/12b. Concentration profiles.
(See Figs 11/12a)

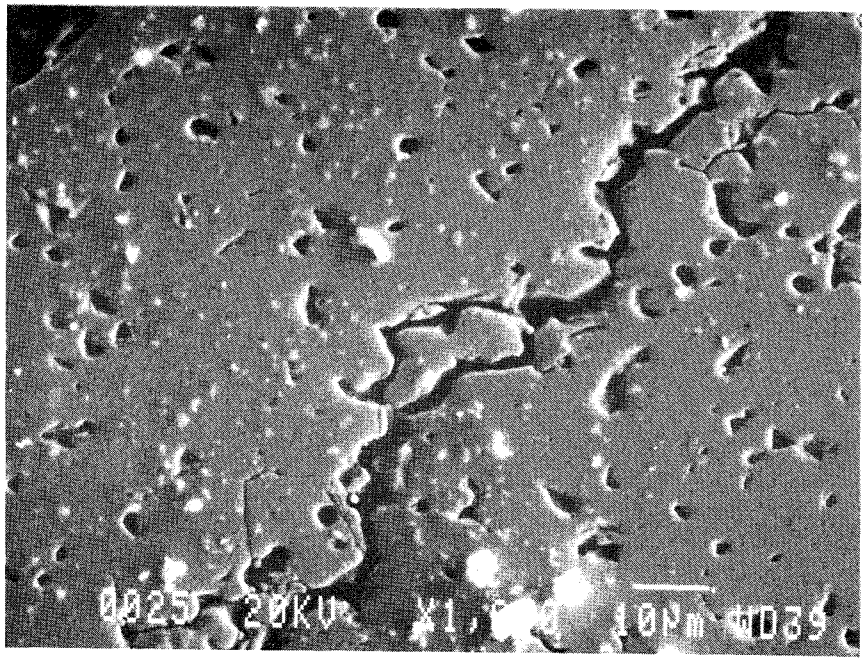

Fig 13. Crack at 2.5 mm from fuel centre showing scanned locations 1 and 2. (See Figs 14 and 15)

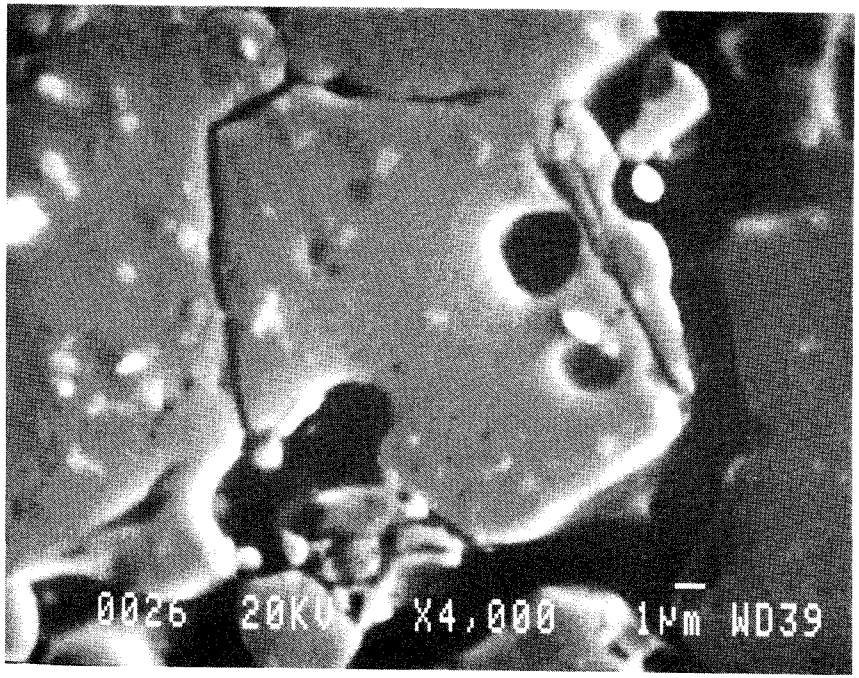

14a. Fuel at crack location 1. (Lower left in Fig 13)

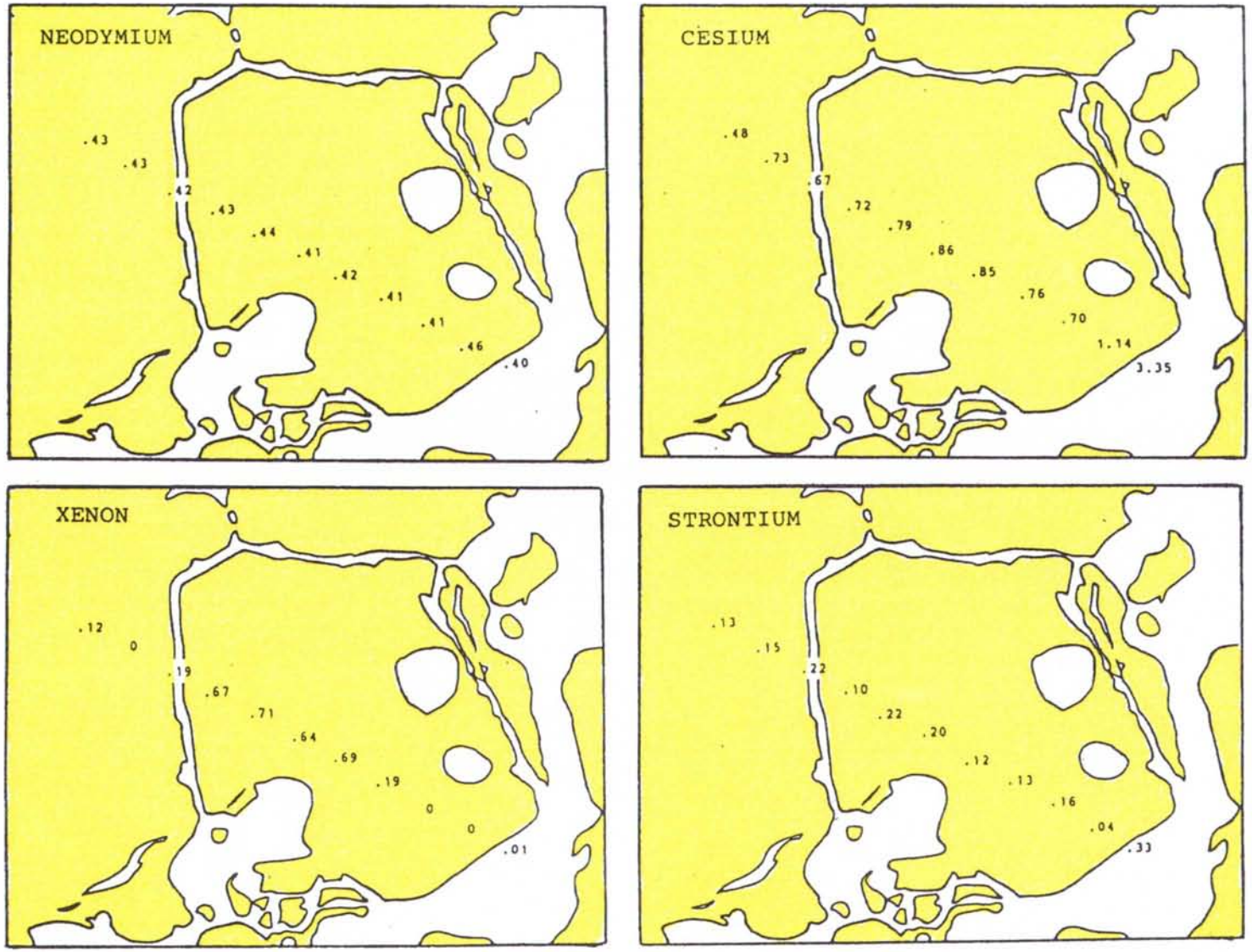

Fig 14b. Concentration maps.
(See Fig 14a)

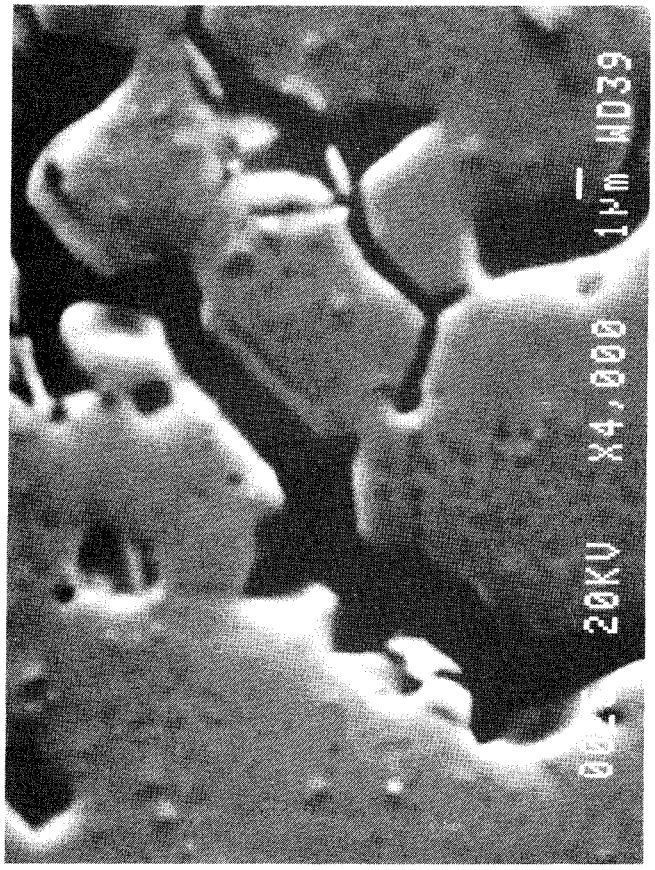

Fig 15a. Fuel at crack location 2.
(Upper right in Fig 13)

Fig 15b. Concentration maps.
(See Fig 15a)

List of SKB reports

Annual Reports

1977–78
TR 121
KBS Technical Reports 1 – 120.
Summaries. Stockholm, May 1979.

1979
TR 79–28
The KBS Annual Report 1979.
KBS Technical Reports 79-01 – 79-27.
Summaries. Stockholm, March 1980.

1980
TR 80–26
The KBS Annual Report 1980.
KBS Technical Reports 80-01 – 80-25.
Summaries. Stockholm, March 1981.

1981
TR 81–17
The KBS Annual Report 1981.
KBS Technical Reports 81-01 – 81-16.
Summaries. Stockholm, April 1982.

1982
TR 82–28
The KBS Annual Report 1982.
KBS Technical Reports 82-01 – 82-27.
Summaries. Stockholm, July 1983.

1983
TR 83–77
The KBS Annual Report 1983.
KBS Technical Reports 83-01 – 83-76
Summaries. Stockholm, June 1984.

1984
TR 85–01
Annual Research and Development Report 1984
Including Summaries of Technical Reports Issued during 1984. (Technical Reports 84-01– 84-19)
Stockholm June 1985.

1985
TR 85-20
Annual Research and Development Report 1985
Including Summaries of Technical Reports Issued during 1985. (Technical Reports 85-01-85-19)
Stockholm May 1986.

1986
TR 86-31
SKB Annual Report 1986
Including Summaries of Technical Reports Issued during 1986
Stockholm, May 1987

1987
TR 87-33
SKB Annual Report 1987
Including Summaries of Technical Reports Issued during 1987
Stockholm, May 1988

Technical Reports

1988

TR 88-01
Preliminary investigations of deep ground water microbiology in Swedish granitic rocks
Karsten Pedersen
University of Göteborg
December 1987

TR 88-02
Migration of the fission products strontium, technetium, iodine, cesium and the actinides neptunium, plutonium, americium in granitic rock
Thomas Ittner[1], Börje Torstenfelt[1], Bert Allard[2]
[1]Chalmers University of Technology
[2]University of Linköping
January 1988

TR 88-03
Flow and solute transport in a single fracture. A two-dimensional statistical model
Luis Moreno[1], Yvonne Tsang[2], Chin Fu Tsang[2], Ivars Neretnieks[1]
[1]Royal Institute of Technology, Stockholm, Sweden
[2]Lawrence Berkeley Laboratory, Berkeley, CA, USA
January 1988

TR 88-04
Ion binding by humic and fulvic acids: A computational procedure based on functional site heterogeneity and the physical chemistry of polyelectrolyte solutions
J A Marinsky, M M Reddy, J Ephraim, A Mathuthu
US Geological Survey, Lakewood, CA, USA
Linköping University, Linköping
State University of New York at Buffalo, Buffalo, NY, USA
April 1987

TR 88-05
Description of geophysical data on the SKB database GEOTAB
Stefan Sehlstedt
Swedish Geological Co, Luleå
February 1988

TR 88-06
Description of geological data in SKBs database GEOTAB
Tomas Stark
Swedish Geological Co, Luleå
April 1988

TR 88-07
Tectonic studies in the Lansjärv region
Herbert Henkel
Swedish Geological Survey, Uppsala
October 1987

TR 88-08
Diffusion in the matrix of granitic rock. Field test in the Stripa mine. Final report.
Lars Birgersson, Ivars Neretnieks
Royal Institute of Technology, Stockholm
April 1988

TR 88-09
The kinetics of pitting corrosion of carbon steel. Progress report to June 1987
G P Marsh, K J Taylor, Z Sooi
Materials Development Division
Harwell Laboratory
February 1988

TR 88-10
GWHRT – A flow model for coupled groundwater and heat flow
Version 1.0
Roger Thunvik[1], Carol Braester[2]
[1] Royal Institute of Technology, Stockholm
[2] Israel Institute of Technology, Haifa
April 1988

TR 88-11
Groundwater numerical modelling of the Fjällveden study site – Evaluation of parameter variations
A hydrocoin study – Level 3, case 5A
Nils-Åke Larsson[1], Anders Markström[2]
[1] Swedish Geological Company, Uppsala
[2] Kemakta Consultants Co, Stockholm
October 1987

TR 88-12
Near-distance seismological monitoring of the Lansjärv neotectonic fault region
Rutger Wahlström, Sven-Olof Linder, Conny Holmqvist
Seismological Depertment, Uppsala University, Uppsala
May 1988

TR 88-13
Validation of the rock mechanics HNFEMP code against Colorado school of mines block test data
Ove Stephansson, Tomas Savilahti
University of Luleå, Luleå
May 1988

TR 88-14
Validation of MUDEC against Colorado school of mines block test data
Nick Barton, Panayiotis Chryssanthakis, Karstein Monsen
Norges Geotekniske Institutt, Oslo, Norge
April 1988

TR 88-15
Hydrothermal effects on montmorillonite. A preliminary study
Roland Pusch
Ola Karnland
June 1988

TR 88-16
Swedish Hard Rock Laboratory
First evaluation of preinvestigations 1986-87 and target area characterization
Gunnar Gustafson
Roy Stanfors
Peter Wikberg
June 1988

TR 88-17
On the corrosion of copper in pure water
T E Eriksen[1], P Ndalamba[1], I Grenthe[2]
[1] The Royal Institute of Technology, Stockholm
Department of nuclear chemistry
[2] The Royal Institute of Technology, Stockholm
Department of inorganic chemistry
March 1988

TR 88-18
Geochemical modelling of the evolution of a granite-concrete-water system around a repository for spent nuclear fuel
Bertrand Fritz, Benoit Madé, Yves Tardy
Université Louis Pasteur de Strasbourg
April 1988

TR 88-19
A Bayesian nonparametric estimation of distributions and quantiles
Kurt Pörn
Studsvik AB
November 1988

TR 88-20

Creep properties of welded joints in OFHC copper for nuclear waste containment

Bo Ivarsson, Jan-Olof Österberg
Swedish Institute for Metals Research
August 1988

TR 88-21

Modelling uranium solubilities in aqueous solutions: Validation of a thermodynamic data base for the EQ3/6 geochemical codes

I Puigdomenech[1], J Bruno[2]
[1]Studsvik Nuclear, Nyköping
Environmental Services
[2]Royal Institute of Technology, Stockholm
Department of Inorganic Chemistry
October 1988

TR 88-22

Radiolysis of ground water: influence of carbonate and chloride on the hydrogen peroxide production

T E Eriksen[1], P Ndalamba[2], H Christensen[2],
E Bjergbakke[3]
[1]The Royal Institute of Technology, Department of Nuclear Chemistry, S-100 44 Stockholm, Sweden
[2]Studsvik Energiteknik AB, S-611 82 Nyköping, Sweden
[3]Risö National Laboratory, DK-4000 Roskilde, Denmark
December 1988

TR 88-23

Source parameters of major earthquakes near Kiruna, northern Sweden, deduced from synthetic seismogram computation

W T Kim, E Skordas, Y P Zohu, O Kulhanek
Seismological Department, Uppsala University,
Box 12019, S-750 12 UPPSALA
June 1988